Tin Monosulfide Thin Films Grown by Atomic Layer Deposition Using Tin 2,4-Pentanedionate and Hydrogen Sulfide

Jay Yu Kim[†,‡] **and Steven M. George***[,†,§]

Department of Chemistry and Biochemistry and Department of Chemical and Biological Engineering, University of Colorado, Boulder, Colorado 80309

Received: December 20, 2009; Revised Manuscript Received: August 15, 2010

Tin monosulfide (SnS) was grown by atomic layer deposition (ALD) using sequential exposures of tin(II) 2,4-pentanedionate ($Sn(acac)_2$) and hydrogen sulfide (H_2S). In situ quartz crystal microbalance (QCM) studies showed that the SnS ALD mass gain per cycle was 11−12 ng/cm^2 at 175 °C on a gold-covered QCM sensor. Using a film density of 5.07 g/cm^3 determined by X-ray reflectivity measurements, these mass gains are equivalent to SnS ALD growth rates of 0.22−0.24 Å/cycle. The ratio of the mass loss and mass gain ($|\Delta m_2/\Delta m_1|$) from the H_2S and $Sn(acac)_2$ reactions was $|\Delta m_2/\Delta m_1| \sim 0.32$ at 175 °C. This measured ratio is close to the predicted ratio from the proposed surface chemistry for SnS ALD. The SnS ALD was self-limiting versus the $Sn(acac)_2$ and H_2S exposures. The SnS ALD growth rate was also independent of substrate temperature from 125 to 225 °C. The SnS ALD growth on Al_2O_3 ALD substrates displayed nucleation problems and smaller growth rates. These differences may be caused by site blocking by the Al(acac)* surface species. X-ray fluorescence studies confirmed a Sn/S atomic ratio of ∼1.0 for the SnS ALD films. X-ray photoelectron spectroscopy measurements revealed that the SnS ALD films contained oxygen impurities at 15−20 atom % after air exposure. These oxygen-containing SnS ALD films displayed a band gap of ∼1.87 eV that is higher than the SnS bulk value of ∼1.3 eV. In addition, these SnS ALD films produced very weak photoluminescence at room temperature. SnS ALD may be useful to fabricate photovoltaic or solar conversion devices.

I. Introduction

Many tin sulfides exist such as SnS, Sn_3S_4, Sn_2S_3, and SnS_2. Tin monosulfide (SnS) is a semiconductor with tin in the Sn(II) oxidation state. SnS is a potentially important photovoltaic and solar conversion material because of its direct optical band gap of ∼1.3 eV.[1] This band gap is similar to silicon and is in the optimum range for solar photoconversion.[2] SnS is also formed from readily available elements and is environmentally benign. Despite these desirable characteristics, very few studies have explored SnS growth and the optical properties of SnS thin films.

There are a variety of methods to deposit SnS films. Several solution methods have been reported for SnS film growth including chemical bath deposition and electrodeposition.[3,4] Vacuum methods of SnS film growth include evaporation and plasma chemical vapor deposition (CVD).[5−7] Tin sulfides have also been deposited by atmospheric pressure CVD using various tin precursors, such as $SnCl_4$ or tri-*n*-butyltin trifluoroacetate, together with hydrogen sulfide.[8,9]

SnS atomic layer deposition (ALD) may be a useful for the fabrication of nanometer-scale thin film photovoltaic or solar conversion devices. ALD is based on sequential, self-limiting surface chemical reactions.[10,11] ALD can provide Ångstrom-level control of the deposited film thickness. ALD also has the ability to provide extremely conformal thin film deposition on high aspect ratio structures.[12] There are no reports of SnS ALD in the literature. However, a recent communication of SnS ALD using a Sn(II) amidinate precursor was presented at the ALD2009 conference.[13] There are other examples of the ALD of metal sulfides such as In_2S_3,[14−18] Cu_xS,[19,20] $InCuS_2$,[21,22] ZnS,[23−25] CdS,[26,27] and PbS.[28−30]

In this paper, SnS ALD was performed using sequential exposures of tin(II) 2,4-pentanedionate ($Sn(acac)_2$) and hydrogen sulfide (H_2S). SnS ALD film growth was investigated using in situ quartz crystal microbalance (QCM) experiments.[31] The SnS ALD films were also studied ex situ using X-ray reflectivity (XRR), X-ray photoelectron spectroscopy (XPS), X-ray fluorescence (XRF) studies, and field emission scanning electron microscopy (FE-SEM). SnS ALD growth rates were measured on various substrates and at different substrate temperatures. SnS ALD films were also grown on glass substrates for optical transmission measurements to characterize the optical band gap and for photoluminescence studies at room temperature.

II. Experimental Section

The SnS ALD growth was performed in a hot wall, viscous flow ALD reactor.[31] A schematic of this reactor is shown in Figure 1. The viscous flow carrier was ultrahigh pure (UHP) nitrogen gas (99.9999%). The continuous flow of N_2 gas at 100 sccm maintained a base pressure of ∼1 Torr in the reactor. The $Sn(acac)_2$ and hydrogen sulfide (H_2S, Aldrich, 99.5+%) were attached to the gas manifold as shown in Figure 1. In addition, trimethylaluminum (TMA) (Aldrich, 97%) and H_2O were also installed on the gas manifold for Al_2O_3 ALD.

The tin(II) 2,4-pentanedionate ($Sn(acac)_2$, Gelest, Inc., 95+%) was placed in a bubbler and heated to ∼105 °C. The $Sn(acac)_2$ was dosed by sending N_2 gas over the headspace of the precursor in the bubbler. TMA, H_2O, and H_2S have vapor pressures of ∼10, ∼20, and >10000 Torr at room temperature, respectively. These precursors can be dosed directly into the N_2 gas flow at

* Corresponding author, Steven.George@Colorado.edu.
† Department of Chemistry and Biochemistry.
‡ Current address: National Renewable Energy Laboratory, Golden, CO 80401.
§ Department of Chemical and Biological Engineering.

10.1021/jp9120244
Published on Web 09/23/2010

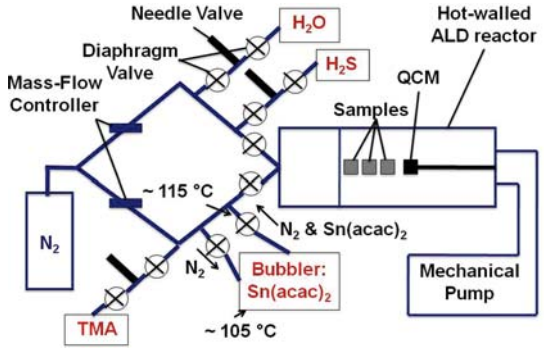

Figure 1. Schematic of the hot wall, viscous flow ALD reactor.

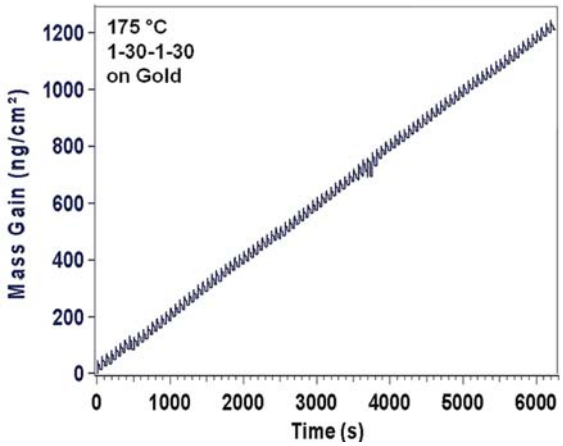

Figure 2. Mass gain versus time for SnS ALD on gold at 175 °C using a pulse sequence of (1−30−1−30) for 100 cycles.

~1 Torr. The pneumatic valves defining the precursor doses were controlled by Labview 7.0. The pressures of the $Sn(acac)_2$ and H_2S doses were ~10 and ~150 mTorr, respectively, as measured by a capacitance manometer on the reactor.

The surface chemistry for SnS ALD is proposed to occur in the following fashion

$$Sn{-}SH^* + Sn(acac)_2 \rightarrow SnS{-}Sn(acac)^* + Hacac \quad (1)$$

$$SnS{-}Sn(acac)^* + H_2S \rightarrow SnSSn{-}SH^* + Hacac \quad (2)$$

where the surface species are marked with asterisks. Reaction 1 exposes the surface to the $Sn(acac)_2$ precursor and converts the SH* surface to an Sn(acac)* surface. Reaction 2 exposes the surface to H_2S and converts the Sn(acac)* surface back to the SH* surface. Following reaction 2, the surface is returned to the original state and is ready for another reaction 1. The repetition of these reactions in an ABAB... sequence will lead to SnS growth in an atomic layer-by-layer fashion.[32]

The SnS ALD films were grown using a pulse sequence of $Sn(acac)_2$, N_2 purge, H_2S, and N_2 purge. This pulse sequence is defined by $(t_1 - t_2 - t_3 - t_4)$ where t_1 is the $Sn(acac)_2$ dose time, t_2 is the N_2 purge time, t_3 is the H_2S dose time, and t_4 is the N_2 purge time. All the times are in seconds. The typical pulse sequence for many of the experiments was (1−30−1−30). The dose times were defined by opening the pneumatic valves.

The QCM experiments of SnS ALD were performed by placing the QCM sensor into the ALD reactor. The QCM sensor is mounted in a Maxtek BSH-150 bakeable sensor housing attached to a 2.75 in. Conflat flange. The sensor housing was altered to provide a N_2 purge of ~20 sccm on the backside of the sensor housing.[31] In addition, Epotek P1011 high-temperature conductive epoxy was used to form a gas-tight, conductive sealing. This N_2 purge and epoxy seal prevented reactant gases from entering the housing and depositing material on the backside of the QCM sensor.[31]

SnS ALD films were also deposited on silicon substrates in the hot wall, viscous flow ALD reactor. Silicon wafers with a native oxide were placed in the reactor. Up to five substrates could be placed on a sample holder. The sample holder was then inserted into the ALD reactor. SnS ALD thin films were grown using a (1−30−1−30) pulse sequence with the silicon substrates at 175 °C.

The XRR scans were performed using a Bede D1 X-ray diffractometer from Bede Scientific, Inc. This X-ray diffractometer was equipped with a Cu X-ray tube and monochromator for Cu Kα radiation at $\lambda = 1.54$ Å. The filament current was 35 mA, and the voltage was 40 kV. Raw data were fit using the REFS fitting software from Bede Scientific, Inc. The XRR fits revealed the film thickness, film density, and surface roughness.

A PHI 5600 X-ray photoelectron spectrometer was used to obtain the XPS of the SnS thin films on gold. Monochromatic Al Kα X-rays at $\lambda = 1486.6$ eV were used for the XPS analysis. Data were collected using Auger Scan (RBD Enterprises, Inc., Bend, OR). XPS data were analyzed using CASA XPS (Casa Software Ltd., U.K.). The X-ray fluorescence was recorded using an X-Calibur energy dispersive XRF spectrometer from Xenemetrix, Inc. FE-SEM images were recorded using JSM-7401F field emission scanning electron microscopy (JEOL Limited).

The optical transmission was measured using a Lambda-950 UV−vis−IR spectrometer equipped with a 4 in. integrating sphere from Perkin-Elmer. The photoluminescence was obtained using a Nanolog system from Horiba Jobin Yvon. This apparatus includes a 532 nm mode-locked frequency-doubled Nd:YAG laser with 8 ps pulses operating at a 78 MHz repetition rate. In addition, an emission spectrometer is employed to resolve spectrally the photoluminescence before detection by a Hamamatsu P2658P photomultiplier tube connected to single-photon counting electronics.

III. Results and Discussion

QCM measurements of mass gain during 100 cycles of SnS ALD on a gold QCM sensor at 175 °C are shown in Figure 2. These results were obtained using a pulse sequence of (1−30−1−30). The mass gain is very linear versus time. The time of one complete SnS ALD cycle is 62 s. The mass gain per one SnS ALD cycle is ~12.0 ng/cm^2. Using a SnS ALD film density of 5.07 g/cm^3 obtained from XRR measurements yields a SnS ALD growth rate of ~0.24 Å per ALD cycle.

An expansion of the QCM results to show three SnS ALD cycles at 175 °C using a pulse sequence of (1−30−1−30) on the gold QCM sensor is displayed in Figure 3. These cycles are the 40th, 41st, and 42nd SnS ALD cycles in Figure 2. The corresponding reactant partial pressures are also shown at the bottom of Figure 3. The partial pressures were ~10 mTorr for the $Sn(acac)_2$ doses and ~150 mTorr for the H_2S doses.

A mass gain of $\Delta m_1 = \sim 18.0$ ng/cm^2 is observed when $Sn(acac)_2$ is dosed for 1 s at 175 °C. This mass gain is related to the adsorption and reaction of $Sn(acac)_2$ on the surface as described in eq 1. The mass gain then decreases slightly during the 30 s N_2 purge. This mass decrease may be related to the

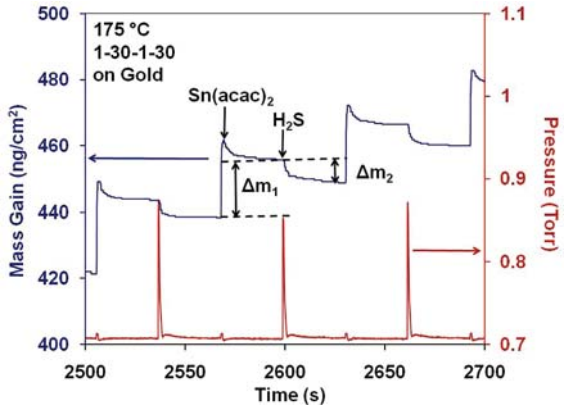

Figure 3. Close-up of the mass gain vs time for three cycles of SnS ALD on gold as shown in Figure 2.

TABLE 1: The Average Mass Gain (Δm_1) and Mass Loss (Δm_2) Resulting from the $Sn(acac)_2$ and H_2S Exposures, Respectively, and the Ratio of the Mass Loss to the Mass Gain, ($|\Delta m_2/\Delta m_1|$), at Different Temperatures[a]

temperature (°C)	Δm_1 (av)	Δm_2 (av)	$\lvert\Delta m_2/\Delta m_1\rvert$
125	19.6	8.0	0.41
150	24.5	11.9	0.49
175	18.2	5.8	0.32
200	12.1	2.0	0.17
225	12.3	2.4	0.20

[a] All the mass changes are given in units of ng/cm^2.

desorption of surface species or some physisorbed $Sn(acac)_2$ precursors on the surface. A mass loss of $\Delta m_2 = \sim -6.0$ ng/cm^2 is then observed during and after the H_2S dose at 175 °C. This mass loss is related to the reaction of H_2S with the surface species as described in eq 2. The mass gain is then constant until the subsequent $Sn(acac)_2$ exposure.

The Δm_1 mass gains and Δm_2 mass losses were measured at a variety of temperatures from 125 to 225 °C. The Δm_1 and Δm_2 mass changes varied with temperature as shown in Table 1. Each mass change was the average of three to five separate experiments. Both the Δm_1 and Δm_2 mass changes decreased at higher temperatures. A lower Δm_1 mass gain is consistent with less $Sn(acac)_2$ reaction and/or more desorption of Sn(acac)* species at the higher temperatures. A lower Δm_2 mass loss is consistent with less H_2S reaction and/or less recombinative desorption of SH* species to produce H_2S at the higher temperatures. However, more recombinative desorption of H_2S would be expected at higher temperatures.

The $|\Delta m_2/\Delta m_1|$ ratios help to determine the surface reaction stoichiometry. Table 1 indicates that the $|\Delta m_2/\Delta m_1|$ ratios decreased at higher temperatures. The ratio was $|\Delta m_2/\Delta m_1| = 0.41$ at 125 °C and reduced to $|\Delta m_2/\Delta m_1| = 0.20$ at 225 °C. These ratios can be compared with the $|\Delta m_2/\Delta m_1|$ ratio predicted from the surface chemistry. On the basis of the $Sn(acac)_2$ and H_2S reactions shown in eqs 1 and 2, the predicted ratio is $|\Delta m_2/\Delta m_1| = 0.30$.

The decreasing Δm_1 and Δm_2 mass changes and $|\Delta m_2/\Delta m_1|$ ratios suggest that the surface chemistry is changing at higher temperatures. The most likely explanation for these decreases is that there is more desorption of Sn(acac)* species that produces smaller Δm_1 mass gains at higher temperatures after the $Sn(acac)_2$ exposures. Fewer remaining Sn(acac)* species would lead to lower Δm_2 mass losses resulting from the H_2S exposures. The decreasing $|\Delta m_2/\Delta m_1|$ ratios also suggest that smaller Sn(acac)* coverages progressively lower the subsequent

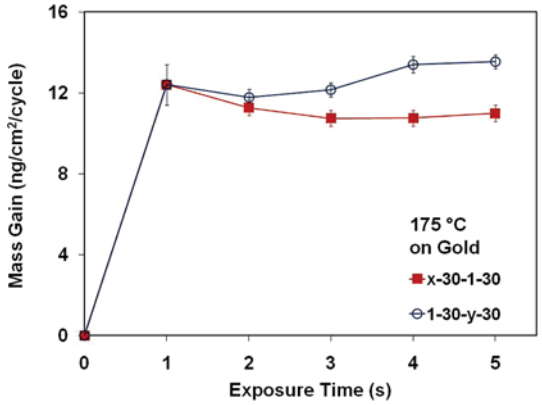

Figure 4. Mass gain per cycle versus $Sn(acac)_2$ or H_2S exposure time for SnS ALD on gold at 175 °C. The H_2S exposure is fixed at 1 s while varying the $Sn(acac)_2$ exposure time using a pulse sequence of (x−30−1−30). The $Sn(acac)_2$ exposure is fixed at 1 s while varying the H_2S exposure time using a pulse sequence of (1−30−y−30).

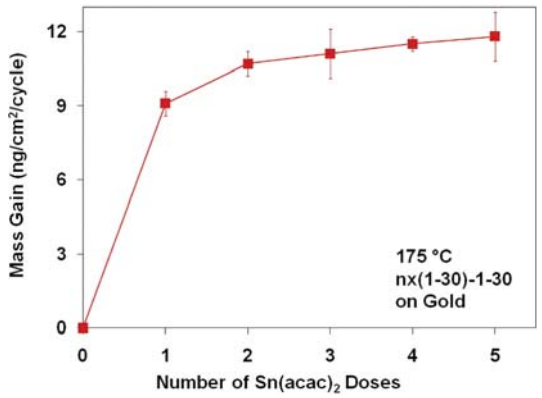

Figure 5. Mass gain per cycle versus number of $Sn(acac)_2$ doses on gold at 175 °C with the H_2S exposure fixed at 1 s using a pulse sequence of (n × (1−30)−1−30).

mass loss resulting from the H_2S reaction. This behavior may be expected if H_2S can remove two Sn(acac)* species at high Sn(acac)* coverage and then only one Sn(acac)* species at lower Sn(acac)* coverages.

Figure 4 shows the mass gain per cycle versus exposure time for $Sn(acac)_2$ and H_2S dose time at 175 °C. In each case, either the $Sn(acac)_2$ or the H_2S dose time is varied while holding the other reactant dose time at 1 s. Each mass gain per cycle is the average of five measurements of 100 cycles of SnS ALD performed for the pulse sequences on a given day. The data points are the averages of the five measurements, and the error bars are the standard deviations. For exposures times ≥1 s, the mass gains per cycle are relatively constant at ∼11−12 ng cm^{-2} cycle^{-1} versus $Sn(acac)_2$ exposure time and ∼12−14 ng cm^{-2} cycle^{-1} versus H_2S exposure time. This behavior indicates that SnS ALD is self-limiting. The surface reactions proceed until the starting reactive functional groups have been converted into the product functional groups. At this point, the surface reaction limits itself because there are no more reactive sites for additional deposition.[32] The slight variations in the mass gain versus exposure time may be caused by day-to-day changes in the experimental parameters.

The self-limiting nature of the $Sn(acac)_2$ exposure is explored further in Figure 5. In this case, the $Sn(acac)_2$ dose time is constant at 1 s and multiple $Sn(acac)_2$ doses are employed to define the total $Sn(acac)_2$ exposure. Each $Sn(acac)_2$ dose of 1 s is followed by a 30 s purge time. Figure 5 shows that the mass gain per cycle is nearly self-limiting versus the number of

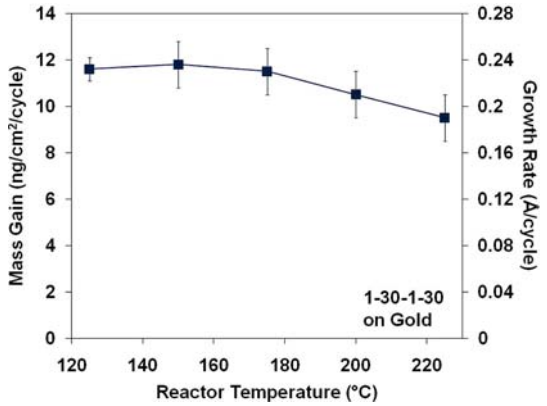

Figure 6. Mass gain per cycle versus reactor temperature for SnS ALD on gold using a pulse sequence of (1−30−1−30).

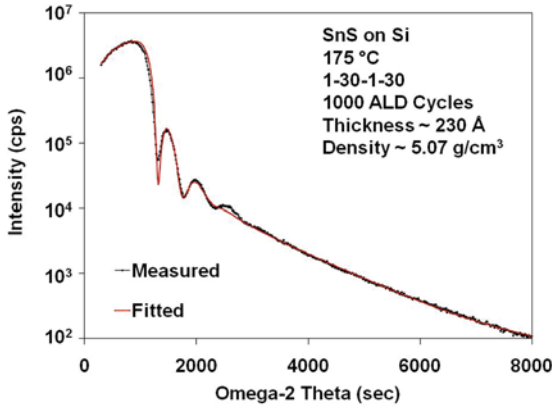

Figure 7. XRR scan showing X-ray intensity vs angle for 1000 cycles of SnS ALD on silicon at 175 °C using a pulse sequence of (1−30−1−30).

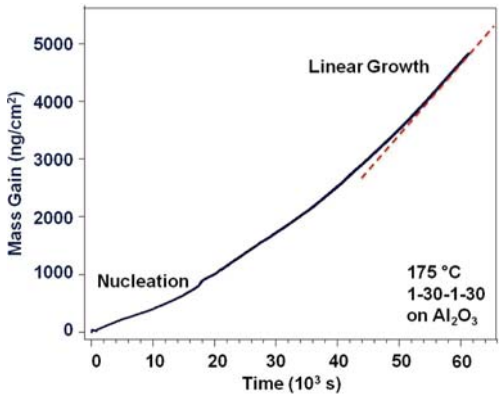

Figure 8. Mass gain vs time for SnS ALD on an Al_2O_3 ALD surface at 175 °C using a pulse sequence of (1−30−1−30).

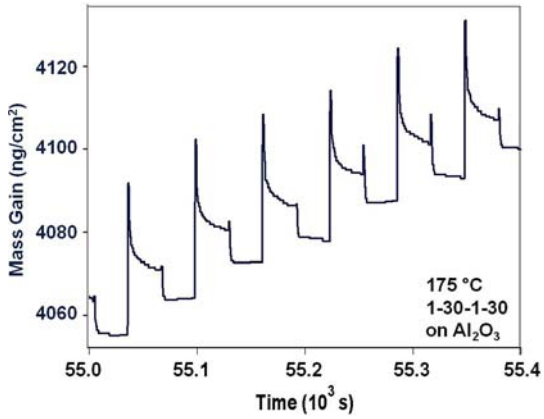

Figure 9. Close up of the mass gain vs time for six cycles of SnS ALD on an Al_2O_3 ALD surface as shown in Figure 8.

$Sn(acac)_2$ doses. The mass gain per cycle reaches a limiting value of ∼11−12 ng cm^{-2} $cycle^{-1}$ after three to four $Sn(acac)_2$ doses. There is good agreement between the results in Figures 4 and 5.

Figure 6 displays the dependence of the mass gain per cycle on the reactor temperature from 125 to 250 °C. Each mass gain per cycle was obtained from 500 cycles of SnS ALD on a separate and new gold QCM sensor. The mass gain per cycle is fairly constant at 11−12 ng cm^{-2} $cycle^{-1}$ for 125−175 °C and then decreases slightly for 200 and 225 °C. This weak temperature dependence for the SnS ALD growth per cycle is different than the previously observed temperature dependence for Cu_xS and In_2S_3 ALD growth per cycle. The growth per cycle for Cu_xS ALD is ∼0.4 Å at 140−200 °C and decreases to 0.2 Å at 200−240 °C.[20] The growth per cycle for In_2S_3 ALD using $In(acac)_3$ and H_2S also decreased more at higher temperatures.[16,33]

Figure 7 shows ex situ XRR measurements for a SnS ALD film on a silicon substrate after 1000 ALD cycles at 175 °C. The XRR measurements yield a SnS film thickness of ∼230 Å with a surface roughness of ∼30 Å. The SnS ALD thickness of 230 Å after 1000 cycles is in good agreement with the growth rate of 0.22−0.24 Å per cycle for SnS ALD at 175 °C. The roughness of ∼30 Å is larger than the expected statistical roughening for a CVD process.[34] Either nucleation difficulties or film crystallinity may be contributing to the surface roughness. XRR also was consistent with a density of the SnS ALD film of 5.07 g/cm^3. This density is very close to the literature value of 5.0 g/cm^3.[35]

The SnS ALD films were also analyzed using FE-SEM. FE-SEM images were obtained for both a clean gold QCM sensor and a SnS ALD film on the gold QCM sensor prepared using 1000 cycles with a pulse sequence of (1−30−1−30) at 175 °C. The surface of the gold QCM sensor appeared a little rough. The FE-SEM image after 1000 cycles of SnS ALD on the gold QCM sensor looked essentially identical. FE-SEM is not able to see any additional roughness features in the SnS ALD film with a thickness of ∼230 Å.

Figure 8 shows the mass gain during 1000 cycles of SnS ALD on an Al_2O_3 ALD film. The Al_2O_3 ALD film was grown using a pulse sequence of (1−30−1−30) for 200 cycles at 175 °C. This pulse sequence was (TMA dose time, N_2 purge time, H_2O dose time, N_2 purge time). The growth per cycle for Al_2O_3 ALD was ∼1.1 Å at 175 °C. The mass gain per cycle for SnS ALD on the Al_2O_3 ALD film is low in the nucleation regime. The growth per cycle during the initial 200 cycles of SnS ALD on Al_2O_3 was only ∼0.05 Å per cycle. The growth per cycle during the last 200 cycles of SnS ALD increases to ∼0.15 Å per cycle. These growth rates on the Al_2O_3 ALD surface are much lower than the growth rates measured on gold or the native oxide on silicon.

Figure 9 shows a close-up of the QCM results in the last 200 cycles of SnS ALD on Al_2O_3 in Figure 8. A comparison of Figures 3 and 9 reveals differences for SnS ALD on gold and Al_2O_3 ALD surfaces. The mass gains are smaller for SnS ALD on Al_2O_3 ALD surfaces. In addition, much larger transients are observed during the $Sn(acac)_2$ doses for SnS ALD on Al_2O_3 ALD surfaces. These transients are consistent mass gains during $Sn(acac)_2$ adsorption and then some mass loss during $Sn(acac)_2$ desorption.

The nucleation difficulties and the lower SnS ALD growth rates on Al_2O_3 ALD substrates may be linked to the poisoning

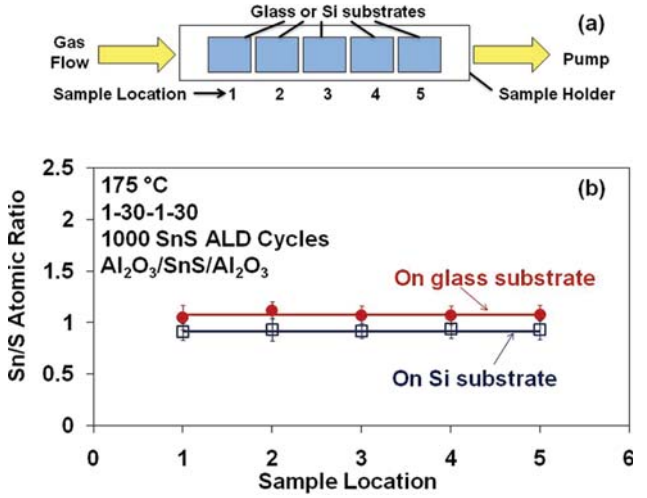

Figure 10. (a) Schematic of substrates at various locations in the ALD reactor. (b) Sn/S atomic ratio determined by XRF analysis for 1000 cycles of SnS ALD on either glass or silicon at 175 °C using a pulse sequence of (1−30−1−30).

of the Al_2O_3 ALD surface by acetylacetonate (acac) ligands from $Sn(acac)_2$. A similar surface poisoning was observed recently during Pd ALD using $Pd(hfac)_2$ and formalin on Al_2O_3 ALD surfaces.[36] Investigations revealed that the Al_2O_3 ALD surface was poisoned by Al(hfac)* species that blocked the reaction sites for Pd ALD. These Al(hfac)* species prevented deposition and led to very low Pd ALD growth rates.[36] Similar Al(acac)* species may form after $Sn(acac)_2$ adsorption that poison the Al_2O_3 ALD surface. In contrast, acac may not form similar tightly bonded species on gold or native oxide silicon surfaces.

To compare the differences between the acac and hexofluoroacetylacetonate (hfac) ligands, preliminary experiments were performed for SnS ALD using tin(II) hexafluoropentanedionate ($Sn(hfac)_2$, Gelest, Inc., 95+%) and H_2S as the reactants on Al_2O_3 ALD substrates. These investigations revealed almost no SnS ALD on the Al_2O_3 ALD surface. These preliminary experiments suggest that the Al(hfac)* species is a very stable site blocker on Al_2O_3 ALD surfaces. The Al(hfac)* species may prevent $Sn(hfac)_2$ from adsorbing on the Al_2O_3 ALD surface.

One possible method to remove the Al(hfac)* or Al(acac)* from the surface is to use TMA to displace the hfac or acac surface species. TMA has been shown to displace the hfac surface species by the reaction: $3Al(hfac)^* + Al(CH_3)_3 \rightarrow Al(hfac)_3 + 3AlCH_3^*$, where the asterisks designate the surface species.[37] This TMA displacement reaction may help improve the nucleation and growth rate for SnS ALD on Al_2O_3 ALD substrates. A similar occurrence of Al(acac)* surface poisoning was suggested in recent studies of In_2S_3 ALD on Al_2O_3 ALD surfaces using $In(acac)_3$ and H_2S.[16]

The spatial uniformity of SnS ALD in the ALD reactor was examined by placing five silicon wafers or glass substrates in the reactor as shown in Figure 10a. These samples were then exposed to 200 cycles of Al_2O_3 ALD using a (1−30−1−30) pulse sequence at 175 °C. Subsequently, SnS ALD was performed using 1000 cycles with a (1−30−1−30) pulse sequence at 175 °C. Another 200 cycles of Al_2O_3 ALD was then placed on the SnS ALD film as a capping layer to minimize any oxidation of the SnS ALD film.

The atomic composition of the SnS ALD films in the Al_2O_3/SnS/Al_2O_3 film stack was investigated using XRF. The ratio of the atomic % of tin and sulfur is shown in Figure 10b. The XRF measurements revealed that the Sn/S atomic ratio was ~1.0 for both the silicon wafers and the glass substrates. In addition, the Sn/S ratio was constant at all locations in the reactor. The samples were slightly sulfur-rich on the silicon wafers and slightly tin-rich on the glass substrates. However, the Sn/S atomic ratios are ~1.0 and nearly the same within experimental variability.

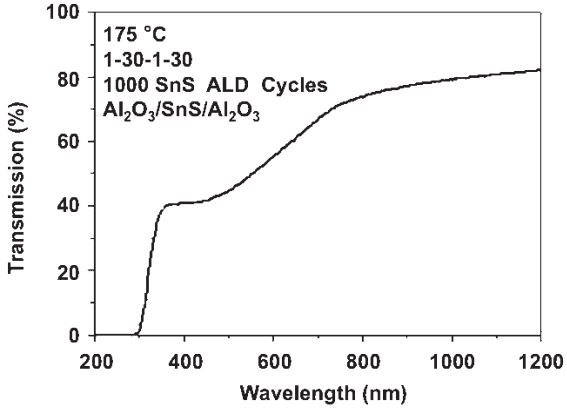

Figure 11. Transmission vs wavelength for an Al_2O_3/SnS/Al_2O_3 film stack. The SnS ALD layer was grown using 1000 cycles of SnS ALD at 175 °C using a pulse sequence of (1−30−1−30).

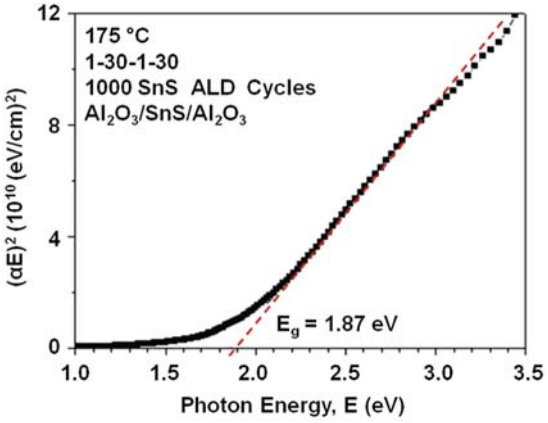

Figure 12. Plot of $(\alpha E)^2$ vs E to deduce the band gap for the SnS ALD films in the Al_2O_3/SnS/Al_2O_3 film stack.

Film thicknesses were also measured for SnS ALD films deposited on Si wafers after 1000 cycles. The SnS ALD films were deposited directly on the native oxide of the Si wafers with no Al_2O_3 ALD interlayer. These Si wafers were placed at different positions in the reactor. The SnS ALD film thicknesses were independent of position in the reactor.

Optical transmission measurements were also performed on the Al_2O_3/SnS/Al_2O_3 film stack deposited on the glass substrates. Figure 11 displays the % transmission from 200 to 1200 nm for the Al_2O_3/SnS/Al_2O_3 film stack. There was no light transmission for wavelengths from 200 to 300 nm. The % transmission then increased to ~40% at ~350 nm. Subsequently, the % transmission steadily increased to ~83% at 1200 nm.

The optical absorption coefficient, α, was calculated from the % transmission curve in Figure 11. α can be calculated from % transmission ($\%T$) as: $\alpha = (1/t)\ \ln(\%T/100)$, where t is the film thickness in centimeters. Plotting α in a number of different manners can help determine whether the band gap is direct or indirect. A plot of $(\alpha E)^2$ versus E (photon energy, eV) is displayed in Figure 12. From this plot, the optical band gap can be deduced from

$$\alpha E = A(E - E_g)^{1/2} \quad (3)$$

In this equation, E_g is the energy band gap and A is a constant. The straight line in Figure 12 indicates that the energy band gap of the SnS ALD film is direct.[6,38−40]

The intercept on the E axis of Figure 12 yields $E_g = 1.87$ eV. This band gap is larger than the bulk value of SnS of ∼1.3 eV.[1] This band gap is also larger than the band gap of 1.6 eV for SnS quantum dots with a diameter of ∼7 nm.[41] The SnS ALD film thickness was not measured by XRR in the $Al_2O_3/SnS/Al_2O_3$ film stack. On the basis of the QCM results in Figure 8, the SnS ALD film thickness in the $Al_2O_3/SnS/Al_2O_3$ film stack is estimated to be ∼94 Å or ∼9.4 nm. Consequently, quantum confinement should not be shifting the band gap to $E_g = 1.87$ eV in the two-dimensional SnS ALD films.

Earlier studies have observed optical band gaps for SnS that are much higher than the bulk SnS value.[6,38,40] The band gaps vary considerably depending on film thickness and deposition temperature. Band gaps have been measured as high as ∼3.5 eV.[40] These results have been explained by the effect of film crystallinity, impurities, and sulfur content.[38] For example, sulfur-rich phases such as SnS_2 and Sn_2S_3 have band gaps >2.0 eV.

Oxygen impurities in the SnS ALD film may also lead to larger than expected band gaps. Low concentrations of oxygen can shift the band gap of β-In_2S_3 from ∼2.1 to ∼2.9 eV in β-$In_2S_{3-3x}O_{3x}$.[42] The shift of the band gap is approximately linear with oxygen concentration and the largest band gap of ∼2.9 eV is obtained with an oxygen concentration of only 8%. Electronic structure calculations reveal that the energy gap increases resulting from compression effects induced by the substitutional oxygen impurities.[42]

XPS measurements were conducted to quantify the oxygen impurities in SnS ALD films after air exposure. These SnS ALD films were prepared with thicknesses of ∼230 Å on gold using 1000 cycles at 175 °C. Before argon sputtering, XPS analysis revealed adventitious carbon and oxygen that may be associated with the carbon. XPS analysis after short sputtering times observed the rapid decrease of the C 1s signal, the reduction of the O 1s signal, and the growth of the Sn 3d and S 2p signals. After sputtering times that removed the C 1s signal, Sn, S, O, and Au were present at ∼25, ∼25, ∼20, and ∼30 atom %, respectively.

The reduction of the O 1s signal relative to the Sn 3d and S 2p signals during sputtering suggests that the SnS ALD film has oxidized from air exposure. Oxidation during SnS ALD growth is unlikely because high-purity N_2 gas (99.9999%) was employed continuously as the carrier gas. The ratio of the mass loss and mass gain from the H_2S and $Sn(acac)_2$ reactions was also close to the predicted ratio from the proposed surface chemistry. The oxidation of the SnS ALD film in air to produce tin oxysulfides or tin oxide is thermochemically predicted because of the greater stability of SnO_2. For example, the reaction $SnS + {}^1/_2O_2 + H_2O \rightarrow SnO_2 + H_2S$ is exothermic with a predicted heat of reaction of $\Delta H = -59$ kcal/mol and free energy change of $\Delta G = -51$ kcal/mol at 20 °C.[43] Oxygen impurities may be producing the larger band gap of the SnS ALD films.

The photoluminescence intensity versus wavelength for the $Al_2O_3/SnS/Al_2O_3$ film stack at room temperature is shown in Figure 13. The excitation wavelength was 532 nm. No photoluminescence was observed when the average excitation power was 5 mW. When the average excitation power was increased to 300 mW, a weak and broad photoluminescence peak appeared at 550−750 nm.

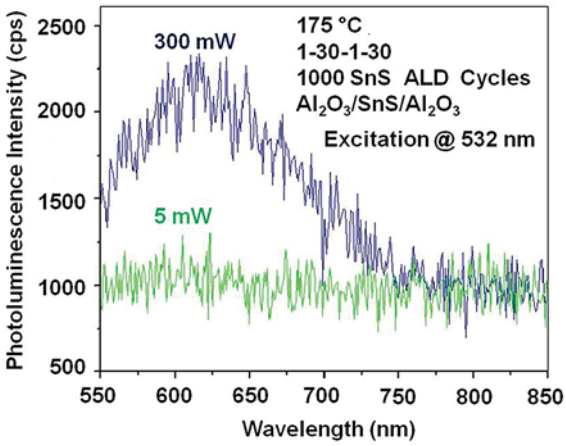

Figure 13. Photoluminescence intensity vs wavelength for the SnS ALD films in the $Al_2O_3/SnS/Al_2O_3$ film stack. The laser excitation at 532 nm was at a power of 5 or 300 mW.

The lack of significant photoluminescence at room temperature is unfortunate for the application of these SnS ALD films as luminescent solar concentrators.[44−48] However, the low photoluminescence at room temperature is not surprising. Sizable photoluminescence yields for semiconductor materials usually occur only at much lower temperatures of <15 K that require liquid helium cooling. Recent work on PbS quantum dots also observed much higher photoluminescence at lower temperatures.[49]

IV. Conclusions

ALD techniques were used to deposit SnS using sequential exposures of $Sn(acac)_2$ and H_2S. QCM measurements determined that the SnS ALD mass gain per cycle was 11−12 ng/cm^2 at 175 °C on gold-covered QCM sensors. These mass gains are equivalent to SnS ALD growth rates of 0.22−0.24 Å/cycle based on a SnS ALD density of 5.07 g/cm^3 measured by XRR analysis. The SnS ALD was self-limiting versus the $Sn(acac)_2$ and H_2S exposures. The SnS ALD growth rate was also nearly temperature independent from 125 to 225 °C. The ratio of the mass loss and mass gain from the H_2S and $Sn(acac)_2$ reactions was close to the predicted ratio from the proposed surface chemistry for SnS ALD.

There were nucleation problems and smaller growth rates for SnS ALD growth on Al_2O_3 ALD surfaces. These differences are believed to be caused by strongly bound acac species on Al_2O_3 and site blocking by the Al(acac)* surface species. X-ray fluorescence studies confirmed a Sn/S atomic ratio of ∼1.0 for the SnS ALD films. The SnS ALD films displayed a large band gap of ∼1.87 eV. This larger band gap may be caused by oxygen impurities in the SnS ALD film resulting from air exposure. The SnS ALD films also displayed very weak photoluminescence at 550−750 nm at room temperature. SnS ALD films will not be effective as a luminescent solar concentrator. However, SnS ALD may find other applications in photovoltaic or solar conversion devices.

Acknowledgment. This research was funded primarily by OmniPV, Inc. The authors thank Dr. Jim Wang and Dr. John Kenny of OmniPV, Inc., for their suggestions and discussions. The XRF measurements were performed at OmniPV, Inc. The optical transmittance and photoluminescence measurements were performed by Professor Kai Shum, Department of Physics, Brooklyn College of CUNY, Brooklyn, NY. Additional support was provided by the National Science Foundation (CHE-

0715552). The authors also thank Dragos Seghete and Andrew S. Cavanagh for their help with the XRR and XPS analysis, respectively.

References and Notes

(1) Reddy, K. T. R.; Reddy, N. K.; Miles, R. W. *Sol. Energy Mater. Sol. Cells* **2006**, *90*, 3041.
(2) Loferski, J. J. *J. Appl. Phys.* **1956**, *27*, 777.
(3) Ichimura, M.; Takeuchi, K.; Ono, Y.; Arai, E. *Thin Solid Films* **2000**, *361*, 98.
(4) Tanusevski, A. *Semicond. Sci. Technol.* **2003**, *18*, 501.
(5) Johnson, J. B.; Jones, H.; Latham, B. S.; Parker, J. D.; Engelken, R. D.; Barber, C. *Semicond. Sci. Technol.* **1999**, *14*, 501.
(6) Miles, R. W.; Ogah, O. E.; Zoppi, G.; Forbes, I. *Thin Solid Films* **2009**, *517*, 4702.
(7) Ortiz, A.; Alonso, J. C.; Garcia, M.; Toriz, J. *Semicond. Sci. Technol.* **1996**, *11*, 243.
(8) Price, L. S.; Parkin, I. P.; Field, M. N.; Hardy, A. M. E.; Clark, R. J. H.; Hibbert, T. G.; Molloy, K. C. *J. Mater. Chem.* **2000**, *10*, 527.
(9) Price, L. S.; Parkin, I. P.; Hardy, A. M. E.; Clark, R. J. H. *Chem. Mater.* **1999**, *11*, 1792.
(10) George, S. M. *Chem. Rev.* **2010**, *110*, 111.
(11) Ritala, M.; Leskela, M. Atomic Layer Deposition. In *Handbook of Thin Film Materials*; Academic Press: San Diego, CA, 2002.
(12) Elam, J. W.; Routkevitch, D.; Mardilovich, P. P.; George, S. M. *Chem. Mater.* **2003**, *15*, 3507.
(13) Sinsermsuksakul, P.; Hock, A. S.; Gordon, R. G. ALD of Tin Monosulfide. *9th International Conference on Atomic Layer Deposition (ALD2009), Monterey, CA*, 2009.
(14) Asikainen, T.; Ritala, M.; Leskela, M. *Appl. Surf. Sci.* **1994**, *82/83*, 122.
(15) Naghavi, N.; Henriquez, R.; Laptev, V.; Lincot, D. *Appl. Surf. Sci.* **2004**, *222*, 65.
(16) Sarkar, S.; Kim, J. Y.; Goldstein, D. N.; Neale, N.; Zhu, K.; Elliott, C. M.; Frank, A. J.; George, S. M. *J. Phys. Chem. C* **2010**, *114*, 8032.
(17) Spiering, S.; Eicke, A.; Hariskos, D.; Powalla, A.; Naghavi, N.; Lincot, D. *Thin Solid Films.* **2004**, *451*, 562.
(18) Yousfi, E. B.; Weinberger, B.; Donsanti, F.; Cowache, P.; Lincot, D. *Thin Solid Films.* **2001**, *387*, 29.
(19) Johansson, J.; Kostamo, J.; Karppinen, M.; Niinisto, L. *J. Mater. Chem.* **2002**, *12*, 1022.
(20) Reijnen, L.; Meester, B.; Goossens, A.; Schoonman, J. *Chem. Vap. Deposition* **2003**, *9*, 15.
(21) Nanu, M.; Reijnen, L.; Meester, B.; Schoonman, J.; Goossens, A. *Chem. Vap. Deposition* **2004**, *10*, 45.
(22) Nanu, M.; Schoonman, J.; Goossens, A. *Adv. Mater.* **2004**, *16*, 453.
(23) Kim, Y. S.; Yun, S. J. *Appl. Surf. Sci.* **2004**, *229*, 105.
(24) Stuyven, G.; De Visschere, P.; Hikavyy, A.; Neyts, K. *J. Cryst. Growth.* **2002**, *234*, 690.
(25) Tammenmaa, M.; Koskinen, T.; Hiltunen, L.; Niinisto, L.; Leskela, M. *Thin Solid Films.* **1985**, *124*, 125.
(26) Han, M.; Luo, Y.; Moryl, J. E.; Osgood, R. M.; Chen, J. G. *Surf. Sci.* **1998**, *415*, 251.
(27) Luo, Y.; Slater, D.; Han, M.; Moryl, J.; Osgood, R. M.; Chen, J. G. *Langmuir.* **1998**, *14*, 1493.
(28) Dasgupta, N. P.; Walch, S. P.; Prinz, F. B. *Electrochem. Soc. Trans.* **2008**, *16*, 29.
(29) Leskela, M.; Niinisto, L.; Niemela, P.; Nykanen, E.; Soininen, P.; Tiitta, M.; Vahakangas, J. *Vacuum* **1990**, *41*, 1457.
(30) Nykanen, E.; Laine-Ylijoki, J.; Soininen, P.; Niinisto, L.; Leskela, M.; Hubert-Pfalzgraf, L. G. *J. Mater. Chem.* **1994**, *4*, 1409.
(31) Elam, J. W.; Groner, M. D.; George, S. M. *Rev. Sci. Instrum.* **2002**, *73*, 2981.
(32) George, S. M.; Ott, A. W.; Klaus, J. W. *J. Phys. Chem.* **1996**, *100*, 13121.
(33) Naghavi, N.; Henriquez, R.; Laptev, V.; Lincot, D. *Appl. Surf. Sci.* **2004**, *222*, 65.
(34) Smith, D. L. *Thin-Film Deposition: Principles and Practice*; McGraw-Hill, Inc.: New York, 1995.
(35) Subramanian, B.; Sanjeeviraja, C.; Jayachandran, M. *Bull. Electrochem.* **2002**, *18*, 349.
(36) Goldstein, D. N.; George, S. M. *Thin Solid Films* Submitted for publication.
(37) Goldstein, D. N.; George, S. M. *Appl. Phys. Lett.* **2009**, *95*, 143106.
(38) Devika, M.; Reddy, N. K.; Ramesh, K.; Ganesan, R.; Gunasekhar, K. R.; Gopal, E. S. R.; Reddy, K. T. R. *J. Electrochem. Soc.* **2007**, *154*, H67.
(39) Ogah, O. E.; Zoppi, G.; Forbes, I.; Miles, R. W. *Thin Solid Films.* **2009**, *517*, 2485.
(40) Reddy, N. K.; Reddy, K. T. R. *Physica B* **2005**, *368*, 25.
(41) Hickey, S. G.; Waurisch, C.; Rellinghaus, B.; Eychmuller., A. *J. Am. Chem. Soc.* **2008**, *130*, 14978.
(42) Robles, R.; Barreau, N.; Vega, A.; Marsillac, S.; Bernede, J. C.; Mokrani, A. *Opt. Mater.* **2005**, *27*, 647.
(43) *HSC Chemistry, 5.11 edition*; Outokumpu Research Oy: Pori, Finland.
(44) Weber, W. H.; Lambe, J. *Appl. Opt.* **1976**, *15*, 2299.
(45) Batchelder, J. S.; Zewail, A. H.; Cole, T. *Appl. Opt.* **1979**, *18*, 3090.
(46) Batchelder, J. S.; Zewail, A. H.; Cole, T. *Appl. Opt.* **1981**, *20*, 3733.
(47) Currie, M. J.; Mapel, J. K.; Heidel, T. D.; Goffri, S.; Baldo, M. A. *Science* **2008**, *321*, 226.
(48) Rowan, B. C.; Wilson, L. R.; Richards, B. S. *IEEE J. Sel. Top. Quantum Electron.* **2008**, *14*, 1312.
(49) Lu, W.; Kamiya, I.; Ichida, M.; Ando, H. *Appl. Phys. Lett.* **2009**, *95*, 083102.

JP9120244